Ballistics of self-jumping microdroplets

Pierre Lecointre,[1,2] Timothée Mouterde,[1,2] Antonio Checco,[3] Charles T. Black,[4] Atikur Rahman,[5] Christophe Clanet,[1,2] and David Quéré[1,2,*]

[1]*Physique et Mécanique des Milieux Hétérogènes, UMR 7636 du CNRS, ESPCI, 75005 Paris, France*
[2]*Laboratoire d'Hydrodynamique de l'X, UMR 7646 du CNRS, École polytechnique, 91128 Palaiseau, France*
[3]*Mechanical Engineering Department, Stony Brook University, Stony Brook, New York 11794, USA*
[4]*Center for Functional Nanomaterials, Brookhaven National Laboratory, Upton, New York 11973, USA*
[5]*Department of Physics, Indian Institute of Science Education and Research (IISER)-Pune, Maharashtra 411008, India*

(Received 5 September 2018; published 7 January 2019)

Water-repellent materials ideally operate at very different liquid scales: from centimeter-size for bugs living on ponds through millimeter-size for antirain functions to micrometer-size for antifogging solids. In the last situation, it was recently evidenced that microdrops condensing on a highly nonadhesive substrate can take advantage from coalescence to jump off the material, even if the dynamical characteristics of the jump were not established at such microscales. We demonstrate in this paper that the jumping speed of drops is nonmonotonic with the drop size, showing a maximum around 5 μm (a size commonly observed in dew), below and above which viscous and inertial effects, respectively, impede the takeoff. We quantitatively describe this optimum in antifogging. We also studied the ballistics of the jumping microdrops, from the height they reached to their behavior at landing; a situation where retakeoff is surprisingly found to be nearly unachievable despite the extreme nonwettability of the material.

DOI: 10.1103/PhysRevFluids.4.013601

I. INTRODUCTION

Water-repellent materials provide a wide variety of functions, which makes them ubiquitous in the natural world. Such materials allow creatures to live at the surface of water [1–3] and they repel water in dynamic conditions (rain) by reflecting impacting millimetric drops [4–6]. These surfaces are also superaerophilic when immersed in water [7], a property that provides oxygen ressources for underwater animals, thermal insulation [8–10], antibiofouling, and slip properties [11–14]. Among these properties, one of the most challenging ones is the ability to repel water at a micrometric scale, that is, at the scale of the texture responsible for superhydrophobicity. However, it was recently shown that nanotextured surfaces may self-remove condensing water [15,16]: growing droplets coalesce and the excess of surface energy can lead to the departure of the resulting drop. Considering that surface energy is converted into kinetic energy, the jumping velocity U of the merged drop scales as $\sqrt{\gamma/\rho r}$, denoting γ as the liquid surface tension, ρ as its density, and r as the radius of the coalescing droplets [15,17,18]. It was first reported that only droplets with radius greater than 10 μm can depart from the substrate [15]. Below this critical radius ($\approx$10 μm), internal viscous dissipation during coalescence was proposed to impede the motion [17,19].

However, recent experimental and numerical studies proved that jumping can occur at a much smaller scale, for $r \approx 5\,\mu$m [20,21], $r \approx 1\,\mu$m [22,23], and even $r \leqslant 500$ nm [18,24–26]. Both this threshold and the jumping velocity are material-dependent [17,19,23,26], and modeling them

*Corresponding author: david.quere@espci.fr

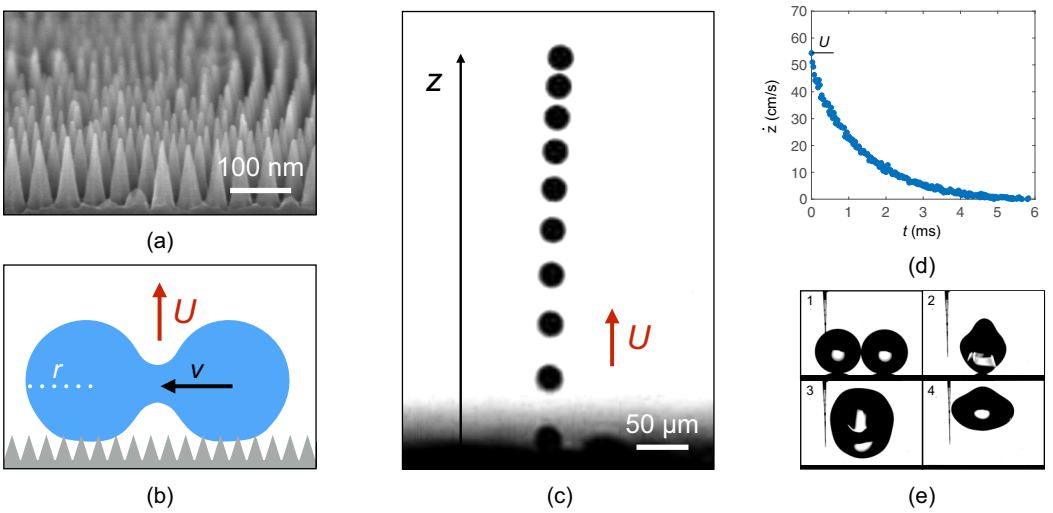

FIG. 1. (a) Scanning electron micrograph of the nanocones used in this study. The scale indicates 100 nm. (b) Sketch of two nonwetting droplets with radius r merging at a velocity v on hydrophobic nanocones; the jumping velocity of the resulting drop is denoted as U. (c) Side-view chronophotography of a jumping drop with radius $R = 11.3 \pm 0.1\,\mu$m resulting from the coalescence of a pair of droplets with $r = 8.9 \pm 0.1\,\mu$m. Images are separated by 0.125 ms. The drop takes off with a vertical jumping velocity $U = 55 \pm 5$ cm/s. (d) Plotting the drop velocity $\dot{z}$ as a function of time t for the experiment of Fig. 1(c) provides our definition of the jumping velocity U: it is taken as the maximum of $\dot{z}$. (e) High-speed photography of a symmetric coalescence of two drops with $r = 580 \pm 5\,\mu$m. Images are separated by 3.7 ms, except the last one which is at 15.5 ms, when the drop reaches its maximum height. The first snapshot (at the top left) shows the beginning of the coalescence while the second one corresponds to takeoff; the measured jumping velocity is $U = 7 \pm 1$ cm/s.

requires to consider both viscous and adhesive effects at such microscales. Our first aim in this paper is to shed light on this issue, based on experiments performed on special textures on which coalescing microdrops systematically take off [22]. We then describe the flight of the expelled drops, from merging and departure to return to the material. In our investigations, we measure the maximum height reached by the jumping water, which in natural cases must be large enough to leave the air boundary layer and to allow the drop to go with the wind, a condition for achieving a genuine antifogging material [16,27–30].

We consider water condensation on a silicon surface covered with nanocones inspired by the textures found on cicada wings [16] [Fig. 1(a)]. These surfaces are fabricated by combining block-copolymer self-assembly with anisotropic plasma etching [31]. The resulting cones have a base diameter of 52 nm and a height of 115 nm, and they are arranged in a dense hexagonal array. Chemical vapor deposition of 1H,1H,2H,2H-perfluorodecyltrichlorosilane makes the surface hydrophobic. This treatment on flat silicon gives an advancing water contact angle $\theta_0 = 120 \pm 2^\circ$, a value that jumps to $\theta_a = 167 \pm 2^\circ$ on the nanocones. The corresponding receding angle is $\theta_r = 157 \pm 2^\circ$, which entails a modest hysteresis $\Delta\theta = \theta_a - \theta_r = 10 \pm 4^\circ$. Condensation of water from the atmosphere is triggered by affixing the substrate on a Peltier module, and setting the temperature at $T_s = 3 \pm 1^\circ$C, a value below the dew point in the laboratory conditions (temperature $T = 25 \pm 1^\circ$C, relative humidity $RH = 39 \pm 1\%$ and supersaturation $S = 1.63 \pm 0.26$).

II. SYMMETRICAL MERGING

Our experiment, sketched in Fig. 1(b), consists of filming the coalescence of pairs of neighboring condensed droplets, simultaneously from above and from aside. Images are captured using

synchronized high-speed videocameras (Photron Fastcam Mini UX100) at a respective rate of 1 and 40 kHz for top and side views, and connected to a microscope (Infinitube In-line and Nikon ELWD 20x). The top view allows us to measure the radii of merging droplets, respectively denoted as r and r' ($r' < r$), and to check that only two-droplet coalescences are considered. We first focus on symmetric merging for which the radii ratio $\varepsilon = r'/r$ is larger than 0.95.

A typical experiment is shown in the chronophotography of Fig. 1(c), where we observe the takeoff of a water drop with radius $R = 11.3 \pm 0.1\,\mu$m resulting from the symmetric coalescence of a pair of droplets with $r = 8.9 \pm 0.1\,\mu$m. Computing the drop position $z(t)$ provides the drop velocity $\dot{z}$ as a function of time [Fig. 1(d)]. The jumping (or departure) velocity U is taken as the maximum of $\dot{z}(t)$. A layer of microdroplets sometimes hides the beginning of the jump, which generates an uncertainty on U on the order of 10%. For the particular case of Figs. 1(c) and 1(d), we measure a jumping velocity $U = 55 \pm 5$ cm/s. We also notice in these figures that the initial acceleration of the drop is extremely strong (with a value on the order of $100g$) and that the small size of the drop makes it highly sensitive to air (quick deceleration, slight deviation from the vertical).

The antifogging ability of our substrate allows us to observe the departure of droplets with radii r spanning from 1.3 to 24 μm [22]. We complemented this interval by also measuring the coalescence of needle-dispensed drops with radii ranging from 150 to 1100 μm. For this second series of experiments, we make our glass needles superhydrophobic by coating them with a Glaco solution (Mirror Coat Zero, Soft99) and drying the solution at 250 °C for half an hour. A first droplet is dispensed from a microneedle and a second one is made the same way until merging occurs, which is recorded from the side at a rate of 4 kHz. The resulting jumping velocity U is obtained as previously, but with larger time steps to filter the interface oscillations. Figure 1(e) shows the takeoff after merging of two drops with radius $r = 580 \pm 5\,\mu$m. The departure velocity is $U = 7 \pm 1$ cm/s, much smaller than observed for smaller drops [Fig. 1(c)]. In addition, we notice strong persistent droplet deformations after coalescence, another consequence of the much larger scale.

The evolution of the jumping velocity U after symmetric coalescence between two drops with radius r is reported in Fig. 2(a). We distinguish two families of data that respectively correspond to condensation ($r \leqslant 24\,\mu$m) and deposition ($r \geqslant 150\,\mu$m). For $r > 5\,\mu$m, U decreases as r increases and the data are well described by the dotted line with slope (0.5 in the log-log plot). "Large" drops depart with the inertiocapillary velocity $U \sim \sqrt{\gamma/\rho r}$, as reported by several authors [15,18,24], a law extended here down to 5 μm. However, drops smaller than 5 μm take off slower than predicted by this scaling and U tends to 0 as r approaches 1 μm, in agreement with the cutoff radius of jumping measured on the same substrate in [22].

The inertiocapillary velocity is generally derived by considering that surface energy is transferred into kinetic energy, an argument that yields $U = (3[2 - 2^{2/3}])^{1/2}\,U^* \approx 1.11U^*$, denoting $U^* = \sqrt{\gamma/\rho r}$. While we observe U scaling as $r^{-1/2}$, this relation overestimates the observed speed by a factor of order 5, as seen in Fig. 2(a), where the law $U = 1.11U^*$ is drawn as a black solid line. Mouterde *et al.* [32] showed that this discrepancy can be removed by expressing the balance of forces during merging. Each droplet retracts at a velocity $v \approx r/\tau$, where $\tau \approx 2\sqrt{\rho r^3/\gamma}$ is the inertiocapillary duration of coalescence. The transfer of momentum can be written $2mU = mv$ [denoting $m = (4\pi/3)\rho r^3$, the mass of each merging droplet], which yields $U = U^*/4$. This velocity has the same scaling form as U^*, but its numerical coefficient is 1/4 instead of 1.11. The best fit coefficient for the data in Fig. 2(a) is 0.22, 10% smaller than 1/4. A possible origin for this slight discrepancy arises from the typical energy $E_a = \pi r^2 \gamma \sin^2\theta_r(1 + \cos\theta_r)$ needed to detach each droplet from the substrate. The corresponding momentum can be written $P_a \approx E_a\tau/r$, which modifies the takeoff velocity in $U = (U^*/4)[1 - 6\sin^2\theta_r(1 + \cos\theta_r)]$. A numerical coefficient of 0.22 corresponds to a receding angle of 154°, a value comparable to the measured angle $\theta_r = 157 \pm 2°$. This small correction in coefficient suggests that water adhesion remains marginal in our system.

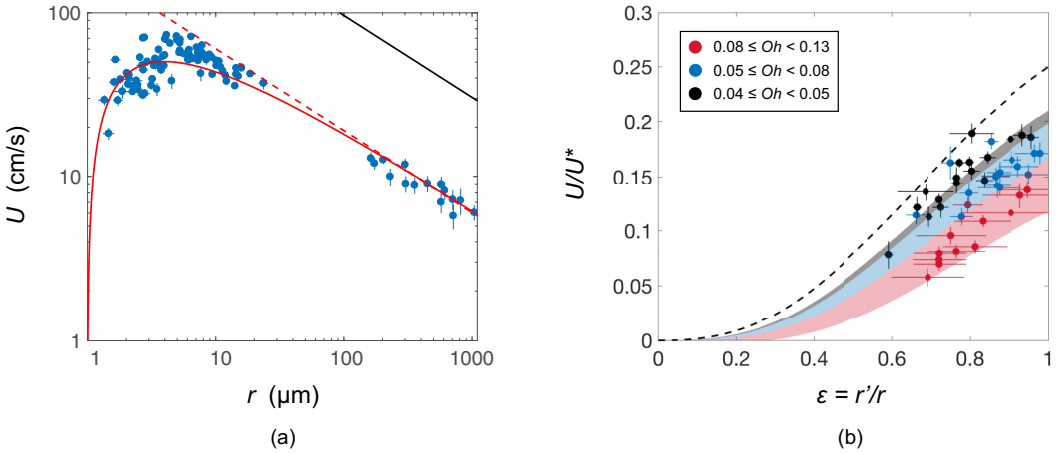

FIG. 2. Jumping velocity resulting from the coalescence of two droplets. (a) Velocity U for symmetric coalescence ($\varepsilon > 0.95$) as a function of the radius r of the two merging drops. Black line shows the speed resulting from energy conservation ($U = 1.11U^*$) and red dashes correspond to $U = 0.22U^*$, denoting $U^* = \sqrt{\gamma/\rho r}$. The red line shows the velocity $U = (U^*/4)\,[\alpha - 4.9\,Oh]$ where $\alpha = 1 - 6\sin^2\theta_r(1 + \cos\theta_r)$ and $Oh = \eta/\sqrt{\rho\gamma r}$ is the Ohnesorge number with η the water viscosity. The coefficient 4.9 is close to 4, the one predicted in Eq. (1). (b) Jumping velocity of droplets after an asymmetric coalescence; U is normalized by $U^* = \sqrt{\gamma/\rho r}$ and plotted as a function of the degree of symmetry $\varepsilon = r'/r$. The three sets of data correspond to three ranges for the larger radius: $2\ \mu\text{m} < r \leqslant 5\ \mu\text{m}$ (red) corresponding to $0.08 \leqslant Oh < 0.13$, $5\ \mu\text{m} < r \leqslant 13\ \mu\text{m}$ (blue) corresponding to $0.05 \leqslant Oh < 0.08$, and $13\ \mu\text{m} < r \leqslant 22\ \mu\text{m}$ (black) corresponding to $0.04 \leqslant Oh < 0.05$. The dashed line shows $U/U^* = \varepsilon^{5/2}/2(1 + \varepsilon^3)$ a function given by momentum conservation and neglecting adhesion and viscous dissipation [32], which provides an asymptotical behavior for the data. Red, blue, and black areas show Eq. (2) drawn with the corresponding colors for each range of Ohnesorge numbers.

The dashes in Fig. 2(a) fairly match the data obtained at "large" radius ($r > 5\ \mu$m), which first suggests that water remains in the Cassie state despite condensation even at microscales [22,33]. Water nuclei growing within conical textures can be brought to the top of the surface by Laplace pressure. A few nanodroplets might remain pinned within the forest of cones, which could explain that the dotted line in Fig. 2(a) slightly overestimates some data in this region. However, adhesion remains marginal at both large and small scales, which explains that about 99% of merging microdroplets take off from nanocones arrays [22].

Conversely, the takeoff velocity U of droplets smaller than $5\,\mu$m strongly deviates from the dashes in Fig. 2(a). In the absence of significant adhesion, we interpret this decrease in mobility by the effect of viscosity. The flow during coalescence generates a dissipative force per droplet $F_v \approx \eta\Delta v\Omega$, where η is the viscosity of water and Ω the droplet volume. Since Δv scales as v/r^2, we deduce $F_v \approx (2\pi\eta/3)(\gamma r/\rho)^{1/2}$, an expression that depends on both viscosity and radius. The resulting loss of momentum $P_v \approx F_v\tau$ is found to be $(4\pi/3)\eta r^2$. For $r \approx 5\ \mu$m and $U \approx 50$ cm/s, the ratio P_v/mU is of order unity and it decreases as $1/\sqrt{r}$, which suggests viscous dissipation as the main cause of loss at microscales. This result qualitatively agrees with numerical simulations that showed that water should be fully immobilized at a scale smaller than 300 nm [18,24].

Taking losses into account, the momentum balance becomes $2mU = mv - 2P_v - 2P_a$, where the factor 2 refers to the number of merging droplets. Hence we get a modified expression for the jumping velocity U:

$$U \approx \frac{U^*}{4}[\alpha - 4Oh], \tag{1}$$

where we introduced the Ohnesorge number $Oh = \eta/(\rho\gamma r)^{1/2}$ and where $\alpha = 1 - 6\sin^2\theta_r(1 + \cos\theta_r)$ is a numerical coefficient close to unity at large θ_r. It is interesting to note that an energy conservation argument leads to a normalized velocity U/U^* scaling as $\sqrt{1 - Oh}$ [17,19,34], a power law different from the one obtained with momentum transfer [Eq. (1)]. Equation (1) is drawn in Fig. 2(a) (red solid line), where $\alpha \approx 0.93$ is not adjusted since it corresponds to the measured value $\theta_r = 157°$; yet we use to best fit the data a coefficient 4.9 instead of 4 in front of the Ohnesorge number, which corrects the coefficient calculated with a scaling argument. We used $\eta = 1.62$ mPa.s, $\rho = 1000\,\mathrm{kg/m^3}$, and $\gamma = 75.3$ mN/m, all quantities considered for water at 3 °C. Equation (1) nicely captures the decrease of the departing velocity for $r \lesssim 5\,\mu$m, i.e., for $Oh \gtrsim 0.1$, showing how viscosity affects the inertiocapillary kinetics. In addition, this expression predicts a critical jumping radius of 1 μm and a maximum jumping velocity U for $r \approx 4\,\mu$m, in good agreement with the experiments. For $r \geqslant 150\,\mu$m, the predicted velocity approaches $U = 0.22U^*$, the asymptotic behavior drawn with a dotted line.

III. ASYMMETRICAL MERGING

Condensing droplets are often asymmetric when they merge due to the randomness of the condensation process. In Fig. 2(b), we plot the reduced takeoff velocity U/U^* as a function of the degree of symmetry $\varepsilon = r'/r$, for different radii r varying between 2 and 22 μm, which makes the Ohnesorge number vary between 0.13 and 0.04. We observe that U/U^* is sensitive both to the Ohnesorge number Oh [as expressed by Eq. (1)], and to the parameter ε: the larger the asymmetry (that is, the smaller ε), the slower the takeoff. A change in ε by typically 25% modifies the jumping velocity by a factor of 2. Hence asymmetry impacts the dynamics of jumping much more than adhesion [found in Eq. (1) to decrease U by only 7%]. For simplicity here, we analyze asymmetry effects by taking $\alpha = 1$ (negligible adhesion). In addition, if we also neglect viscosity, we can write the transfer of momentum as $(m + m')U = m'v'$, denoting $v' \approx r'/\tau'$ and $\tau' \approx 2\sqrt{\rho r'^3/\gamma}$ as the merging velocity and time of the smaller droplet. This yields $U = U^*\varepsilon^{5/2}/2(1 + \varepsilon^3)$ [32], a prediction drawn with a dashed line in Fig. 2(b). This behavior is found to capture asymptotically the data at large r (black symbols). Smaller droplets are slower, which we understand mostly as a consequence of the viscous dissipation described above. We generalize Eq. (1) to the case of asymmetric merging by rewriting the momentum balance as $(m + m')U = m'v' - P'_\mathrm{v} - P_\mathrm{v}$, using the same notations as previously. On the one hand, we have $P'_\mathrm{v} \approx F'_\mathrm{v}\tau'$, where the viscous force $F'_\mathrm{v} \approx \eta\Delta v'\Omega'$ is integrated over the merging time τ'. On the other hand, we assume $P_\mathrm{v} = P'_\mathrm{v}$ because the small drop induces fluid motion in the large one at its own scale, as shown in simulations by Eiswirth *et al.* [35]. Hence, we get an analytical expression for the jumping velocity U in an asymmetric configuration:

$$U \approx U^*\left[\frac{\varepsilon^{5/2}}{2(1+\varepsilon^3)} - 2Oh\frac{\varepsilon^2}{1+\varepsilon^3}\right]. \tag{2}$$

Despite the small size of the droplets, the Ohnesorge number $Oh = \eta/(\rho\gamma r)^{1/2}$ remains small (<0.2), so that U/U^* simply increases with ε at fixed r, and with r at fixed ε, as observed in Fig. 2(b). As asymmetry vanishes ($\varepsilon \to 1$), Eq. (2) reduces to Eq. (1) (with $\alpha = 1$ since we neglected adhesion). Drawn in Fig. 2(b) for three ranges of increasing radii, that is, three ranges of Oh (red, blue, and black areas), Eq. (2) is observed to show a fair agreement with the data. More generally, it describes how the conjunction of asymmetry and microscale affects drop departure, a key feature for understanding and tailoring the efficiency of antifogging materials.

IV. DROPLET FLIGHT AND LANDING

After takeoff, drops follow quasivertical paths [Fig. 1(c)] until falling back to the substrate. We discuss here the flight of microdrops ($r \leqslant 17\,\mu$m) formed after coalescence. We denote their radius

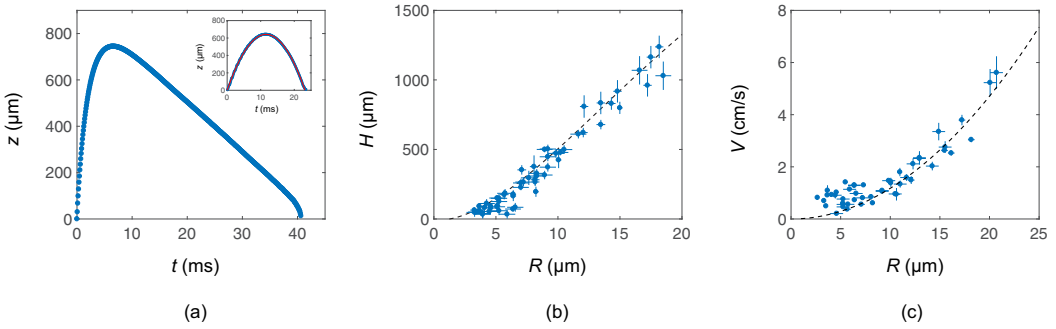

FIG. 3. Flight of departing drops after takeoff. (a) Vertical trajectory $z(t)$ of a drop with radius $R = 12.9 \pm 0.7$ μm after its ejection at a velocity $U = 29 \pm 2$ cm/s. Inset: Same plot for a drop with radius $R = 287 \pm 3$ μm departing at $U = 11 \pm 2$ cm/s. The function $z(t)$ is nicely fitted by a parabola (red solid line). (b) Maximum measured height H reached during flight as a function of radius R. The dashed line represents the theoretical height $H = U\tau_a - g\tau_a^2 \ln(1 + U/g\tau_a)$. (c) Absolute terminal velocity V as a function of radius R. The dashed line corresponds to the velocity given by the equilibrium between gravity and Stokes drag $V = (2/9)\rho g R^2/\eta_a$.

as $R = (r^3 + r'^3)^{1/3}$ (volume conservation), and we report in Fig. 3(a) the temporal evolution $z(t)$ for a drop with radius $R = 12.9 \pm 0.7$ μm departing at $U = 29 \pm 2$ cm/s. The function $z(t)$ is observed to be highly asymmetric. While the ascending phase occupies 20% of the flight time, the descending phase takes much longer, a consequence of the action of air viscosity at microscales. This friction is also responsible for the modest maximum height ($H = 740$ μm) reached by the drop after less than 6 ms. The Reynolds number in air is $\mathrm{Re} = \rho_a U R/\eta_a$, with U the jumping velocity, ρ_a and η_a the air density and viscosity. At microscales, Re is smaller than unity and Stokes drag $F = 6\pi\eta_a R\dot{z}$ is the main source of friction [24]. Hence the successive phases of rise and descent can be expressed by a balance between drag, inertia, and gravity, which yields the speed $\dot{z}$ as a function of time t:

$$\dot{z}(t) = (U + g\tau_a)e^{-t/\tau_a} - g\tau_a, \tag{3}$$

where the braking time τ_a is equal to $(2/9)\rho R^2/\eta_a$ [36]. Microdrops ballistics markedly differs from that of drops larger than 100 μm. For these, the drag force becomes negligible, which classically yields the parabolic motion resulting from a balance between inertia and gravity. The inset in Fig. 3(a) shows it for a drop with radius $R = 287 \pm 3$ μm departing at $U = 11 \pm 1$ cm/s, together with its parabolic fit drawn in red.

From our observations, we can also extract a useful, practical quantity, namely the maximum height H reached by the drop and plotted in Fig. 3(b) [27–29]. Integrating Eq. (3) yields $z(t) = \tau_a(U + g\tau_a)(1 - e^{-t/\tau_a}) - g\tau_a t$, whose maximum is:

$$H = U\tau_a - g\tau_a^2 \ln\left(1 + \frac{U}{g\tau_a}\right). \tag{4}$$

The main parameter in the last equation is the radius R, both contained in the departing velocity U [Eq. (1)] and in the braking time τ_a [Eq. (3)]. At microscales, τ_a is small so that H increases with R, as $R^{3/2}$. Equation (4) predicts that $H(R)$ reaches a maximum around $R \approx 50$ μm, a size larger than that of condensing drops. Drawn with a dashed line in Fig. 3(b) without adjustable parameter, Eq. (4) nicely describes the data. In the presence of a wind, in the range of 1–10 m/s, the air boundary layer at a centimeter size solid surface expelling dew has a thickness of about 100 μm, showing that most drops can escape this layer and be entrained by the wind (an interesting property if the substrate is horizontal for avoiding the redeposition of dew). For vertical substrates,

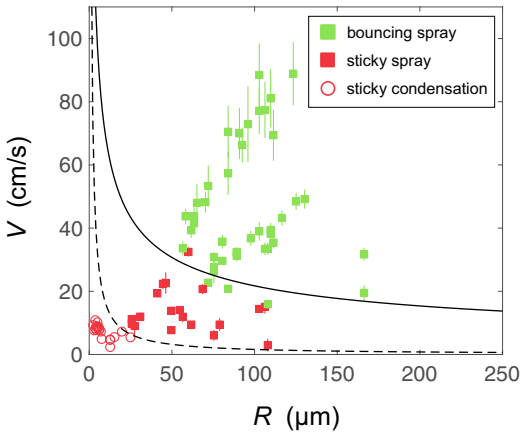

FIG. 4. Phase diagram of droplets at landing. The drop radius and velocity are denoted as R and V. Green color indicates bouncing and red color indicates sticking. Dots and squares mean that drops are made from condensation or from a spray, respectively. The solid line expresses the balance between adhesion and inertia [Eq. (5)]. The dashed line represents the threshold of bouncing dictated by viscosity $V^* \approx \eta/\rho R$.

H is the typical distance of ejection, after which droplets can fall under the action of gravity. This quantity is also useful to size the so-called phase-change thermal diodes (rectifying heat transfer [37]) by fixing the maximum gap for which jumping drops can be collected by a solid plate above the jumping stage.

On descent, drops quickly reach their terminal velocity V, plotted in Fig. 3(c) as a function of the radius R and compared to the prediction $V = g\tau_a$ (dashed line). The fit is convincing except at small radius ($R \leqslant 8\,\mu$m) where V can be as much as ten times larger than predicted. This discrepancy may originate from a charge effect [38] adding an electrostatic attractive contribution to the force balance, which is dominant at small substrate distances (i.e., at small R). This supplementary attraction is found to become significant at a distance of about 200 μm, which corresponds [in Fig. 3(b)] to a radius of about 7.5 μm, the size below which the gravitational prediction does not apply.

Droplets finally return to the substrate, which they impact at the velocity V. We study the landing for both condensed drops ($2.7\,\mu\text{m} \leqslant R \leqslant 22.7\,\mu\text{m}$ and $2\text{ cm/s} \leqslant V \leqslant 15\text{ cm/s}$) and water sprayed onto the surface ($25\,\mu\text{m} \leqslant R \leqslant 160\,\mu\text{m}$ and $2\text{ cm/s} \leqslant V \leqslant 100\text{ cm/s}$), and report in Fig. 4 the behavior of drops after impact: Either they bounce (green data), as expected on a repellent material, or they stick [red data split between sprayed (squares) and condensed droplets (empty circles)]. Only drops with large size R and velocity V are observed to bounce. Conversely, none of the droplets formed by condensation get reflected by the material from which they were ejected: Dew repellency is found to be more demanding than dew ejection, on which we now comment.

Our experiments probe the very unusual situation of microdrops impacting a solid at a small velocity (red circles). The corresponding Reynolds number $\text{Re} = \rho RV/\eta$ is of order unity or even smaller. Therefore, even in the limit of a strictly nonadhesive material ($\theta_r = 180^\circ$), drops should stick when the viscous dissipation at impact exceeds the kinetic energy. $\text{Re} = 1$ provides the threshold $V^* = \eta/\rho R$ above which we leave this regime. This frontier is marked with a dashed line in Fig. 4 and it is found to enclose all the data for dew. Being above this dashed line does no guarantee bouncing either. The Weber number $We = \rho V^2 R/\gamma$ controlling liquid deformation at impact in this domain remains modest, on the order of 0.1. Hence, for the sake of simplicity we consider that impacting water contacts the substrate with a radius of order R, with a contact line dissipation of order $\pi R^2\gamma(1 + \cos\theta_r)$. Drops will stick if this quantity exceeds the kinetic energy at impact $2\pi R^3\rho V^2/3$. The balance between these two energies yields a minimum velocity V^*

required for repellency:

$$V^* \approx \sqrt{\frac{3\gamma}{2\rho R}(1+\cos\theta_r)}. \tag{5}$$

Drawn with a solid line in Fig. 4, Eq. (5) nicely captures the frontier between bouncing and sticking. More generally, if we model the behavior of droplets after ejection using Eq. (3), we find $g\tau_a > V^*$ as a criterion for bouncing. Both the dependencies of τ_a and V^* with R being known, we deduce a minimum radius for bouncing $R^* = [243\,\eta_a^2\,\gamma\,(1+\cos\theta_r)/8\rho^3 g^2]^{1/5}$, a quantity around 60 μm. Such drops are larger than that obtained after condensation, which confirms the unability of condensed drops to bounce. It may seem surprising that an antifogging surface is unable to reflect the water ejected from it, but this is mainly a consequence of their slowness at impact. The only possibility for such a drop to bounce is to meet another one at impact [39,40].

V. SUMMARY

In summary, we provide quantitative measurements of the jumping velocity of coalescing droplets with radii ranging from 1 μm to 1 mm. Experiments at small scales are made possible by the use of highly nonadhesive materials, which enables water to remain mobile even at microscale. We report that the jumping velocity obeys the classical inertiocapillary scaling down to 5 μm, below which strong deviations are observed and interpreted as a consequence of viscous dissipation. The asymmetry of merging is shown to be another cause of reduced jumping efficiency. We characterize the flight, maximum height, descent kinetics, and landing of jumping microdroplets. Air viscosity rapidly stops ejected drops that later fall so slowly that they cannot bounce after impact. Our findings might help to design new antifogging properties where condensation produces drops large enough to be efficiently evacuated from the surface. The coupling of this motion with a lateral wind would be interesting to study, as well as the case where drops take off with solid particles (contamination or ballistospore) [41–44]. Another natural development of this study would be to understand how more than two drops merging on the surface are ejected.

ACKNOWLEDGMENTS

We thank Julien Husson and Alexandra Zak for the fabrication of the glass microneedles. Research carried out at Brookhaven National Laboratory is supported by the US Department of Energy, Office of Basic Energy Sciences, under Contract No. DE-AC02-98CH10886 and used resources of the Center for Functional Nanomaterials, which is a U.S. DOE Office of Science Facility. P.L. thanks the Ecole polytechnique for the financial support (Monge Fellowship). T.M. thanks the Direction Générale de l'Armement (DGA) for contributing to the financial support, Rose-Marie Sauvage and Thierry Midavaine for their constant interest, and Thales for cofunding this project. Finally, we thank Romain Labbé for help in the design of the experiments.

[1] D. L. Hu, B. Chan, and J. W. M. Bush, The hydrodynamics of water strider locomotion, Nature **424**, 663 (2003).
[2] X. Gao and L. Jiang, Biophysics: water-repellent legs of water striders, Nature **432**, 36 (2004).
[3] J. W. M. Bush and D. L. Hu, Walking on water: biolocomotion at the interface, Annu. Rev. Fluid Mech. **38**, 339 (2006).
[4] R. Blossey, Self-cleaning surfaces—virtual realities, Nat. Mater. **2**, 301 (2003).
[5] J. C. Bird, R. Dhiman, H.-M. Kwon, and K. K. Varanasi, Reducing the contact time of a bouncing drop, Nature **503**, 385 (2013).

[6] Y. Liu, L. Moevius, X. Xu, T. Qian, J. M. Yeomans, and Z. Wang, Pancake bouncing on superhydrophobic surfaces, Nat. Phys. **10**, 515 (2014).
[7] C. Shi, X. Cui, X. Zhang, P. Tchoukov, Q. Liu, N. Encinas, M. Paven, F. Geyer, D. Vollmer, Z. Xu, H.-J. Butt, and H. Zeng, Interaction between air bubbles and superhydrophobic surfaces in aqueous solutions, Langmuir **31**, 7317 (2015).
[8] W. A. Calder, Temperature relations and underwater endurance of the smallest homeothermic diver, the water shrew, Comp. Biochem. Physiol. **30**, 1075 (1969).
[9] M. R. Flynn and J. W. M. Bush, Underwater breathing: the mechanics of plastron respiration, J. Fluid Mech. **608**, 275 (2008).
[10] A. Balmert, H. F. Bohn, P. Ditsche-Kuru, and W. Barthlott, Dry under water: Comparative morphology and functional aspects of air-retaining insect surfaces, J. Morphol. **272**, 442 (2011).
[11] C. Cottin-Bizonne, J.-L. Barrat, L. Bocquet, and E. Charlaix, Low-friction flows of liquid at nanopatterned interfaces, Nat. Mater. **2**, 237 (2003).
[12] J. Ou, B. Perot, and J. P. Rothstein, Laminar drag reduction in microchannels using ultrahydrophobic surfaces, Phys. Fluids **16**, 4635 (2004).
[13] A. Tuteja, W. Choi, M. Ma, J. M. Mabry, S. A. Mazzella, G. C. Rutledge, G. H. McKinley, and R. E. Cohen, Designing superoleophobic surfaces, Science **318**, 1618 (2007).
[14] A. Steele, I. Bayer, and E. Loth, Inherently superoleophobic nanocomposite coatings by spray atomization, Nano Lett. **9**, 501 (2008).
[15] J. B. Boreyko and C.-H. Chen, Self-Propelled Dropwise Condensate on Superhydrophobic Surfaces, Phys. Rev. Lett. **103**, 184501 (2009).
[16] K. M. Wisdom, J. A. Watson, X. Qu, F. Liu, G. S. Watson, and C.-H. Chen, Self-cleaning of superhydrophobic surfaces by self-propelled jumping condensate, Proc. Natl. Acad. Sci. U.S.A. **110**, 7992 (2013).
[17] C. Lv, P. Hao, Z. Yao, Y. Song, X. Zhang, and F. He, Condensation and jumping relay of droplets on lotus leaf, Appl. Phys. Lett. **103**, 021601 (2013).
[18] F. Liu, G. Ghigliotti, J. J. Feng, and C.-H. Chen, Numerical simulations of self-propelled jumping upon drop coalescence on non-wetting surfaces, J. Fluid Mech. **752**, 39 (2014).
[19] F.-C. Wang, F. Yang, and Y.-P. Zhao, Size effect on the coalescence-induced self-propelled droplet, Appl. Phys. Lett. **98**, 053112 (2011).
[20] R. Enright, N. Miljkovic, J. Sprittles, K. Nolan, R. Mitchell, and E. N. Wang, How coalescing droplets jump, ACS Nano **8**, 10352 (2014).
[21] M.-K. Kim, H. Cha, P. Birbarah, S. Chavan, C. Zhong, Y. Xu, and N. Miljkovic, Enhanced jumping-droplet departure, Langmuir **31**, 13452 (2015).
[22] T. Mouterde, G. Lehoucq, S. Xavier, A. Checco, C. T. Black, A. Rahman, T. Midavaine, C. Clanet, and D. Quéré, Antifogging abilities of model nanotextures, Nat. Mater. **16**, 658 (2017).
[23] M. D. Mulroe, B. R. Srijanto, S. F. Ahmadi, C. P. Collier, and J. B. Boreyko, Tuning superhydrophobic nanostructures to enhance jumping-droplet condensation, ACS Nano **11**, 8499 (2017).
[24] F. Liu, G. Ghigliotti, J. J. Feng, and C.-H. Chen, Self-propelled jumping upon drop coalescence on Leidenfrost surfaces, J. Fluid Mech. **752**, 22 (2014).
[25] Z. Liang and P. Keblinski, Coalescence-induced jumping of nanoscale droplets on super-hydrophobic surfaces, Appl. Phys. Lett. **107**, 143105 (2015).
[26] H. Cha, C. Xu, J. Sotelo, J. M. Chun, Y. Yokoyama, R. Enright, and N. Miljkovic, Coalescence-induced nanodroplet jumping, Phys. Rev. Fluids **1**, 064102 (2016).
[27] B. Peng, S. Wang, Z. Lan, W. Xu, R. Wen, and X. Ma, Analysis of droplet jumping phenomenon with lattice Boltzmann simulation of droplet coalescence, Appl. Phys. Lett. **102**, 151601 (2013).
[28] G. S. Watson, M. Gellender, and J. A. Watson, Self-propulsion of dew drops on lotus leaves: a potential mechanism for self cleaning, Biofouling **30**, 427 (2014).
[29] G. S. Watson, L. Schwarzkopf, B. W. Cribb, S. Myhra, M. Gellender, and J. A. Watson, Removal mechanisms of dew via self-propulsion off the gecko skin, J. R. Soc., Interface **12**, 20141396 (2015).

[30] J. Liu, H. Guo, B. Zhang, S. Qiao, M. Shao, X. Zhang, X.-Q. Feng, Q. Li, Y. Song, L. Jiang, and J. Wang, Guided self-propelled leaping of droplets on a micro-anisotropic superhydrophobic surface, Angew. Chem. **128**, 4337 (2016).
[31] A. Checco, A. Rahman, and C. T. Black, Robust superhydrophobicity in large-area nanostructured surfaces defined by block-copolymer self assembly, Adv. Mater. **26**, 886 (2014).
[32] T. Mouterde, T.-V. Nguyen, H. Takahashi, C. Clanet, I. Shimoyama, and D. Quéré, How merging droplets jump off a superhydrophobic surface: Measurements and model, Phys. Rev. Fluids **2**, 11200 (2017).
[33] B. Zhang, X. Chen, J. Dobnikar, Z. Wang, and X. Zhang, Spontaneous wenzel to cassie dewetting transition on structured surfaces, Phys. Rev. Fluids **1**, 073904 (2016).
[34] H. Vahabi, W. Wang, S. Davies, J. M. Mabry, and A. K. Kota, Coalescence-induced self-propulsion of droplets on superomniphobic surfaces, ACS Appl. Mater. Interfaces **9**, 29328 (2017).
[35] R. Eiswirth, H.-J. Bart, A. Ganguli, and E. Kenig, Experimental and numerical investigation of binary coalescence: Liquid bridge building and internal flow fields, Phys. Fluids **24**, 062108 (2012).
[36] See Supplemental Material at http://link.aps.org/supplemental/10.1103/PhysRevFluids.4.013601 for the related content and supplementary movies.
[37] J. B. Boreyko, Y. Zhao, and C.-H. Chen, Planar jumping-drop thermal diodes, Appl. Phys. Lett. **99**, 234105 (2011).
[38] N. Miljkovic, D. J. Preston, R. Enright, and E. N. Wang, Electrostatic charging of jumping droplets, Nat. Commun. **4**, 2517 (2013).
[39] C. Lv, P. Hao, Z. Yao, and F. Niu, Departure of condensation droplets on superhydrophobic surfaces, Langmuir **31**, 2414 (2015).
[40] X. Chen, R. S. Patel, J. A. Weibel, and S. V. Garimella, Coalescence-induced jumping of multiple condensate droplets on hierarchical superhydrophobic surfaces, Sci. Rep. **6**, 18649 (2016).
[41] J. Turner and J. Webster, Mass and momentum transfer on the small scale: How do mushrooms shed their spores? Chem. Eng. Sci. **46**, 1145 (1991).
[42] A. Pringle, S. N. Patek, M. Fischer, J. Stolze, and N. P. Money, The captured launch of a ballistospore, Mycologia **97**, 866 (2005).
[43] X. Noblin, S. Yang, and J. Dumais, Surface tension propulsion of fungal spores, J. Exp. Biol. **212**, 2835 (2009).
[44] F. Liu, R. L. Chavez, S. Patek, A. Pringle, J. J. Feng, and C.-H. Chen, Asymmetric drop coalescence launches fungal ballistospores with directionality, J. R. Soc., Interface **14**, 20170083 (2017).